

Review

# A Review of the Application of Modified Separators in Inhibiting the “shuttle effect” of Lithium–Sulfur Batteries

Bo-Wen Zhang <sup>1</sup>, Bo Sun <sup>2</sup>, Pei Fu <sup>1</sup>, Feng Liu <sup>1</sup>, Chen Zhu <sup>1</sup>, Bao-Ming Xu <sup>1</sup>, Yong Pan <sup>1</sup> and Chi Chen <sup>1,\*</sup>

<sup>1</sup> Hubei Provincial Key Laboratory of Green Materials for Light Industry, Hubei University of Technology, Wuhan 430068, China

<sup>2</sup> Shandong Zhongsheng Pharmaceutical Equipment Co., Ltd., Yantai 264010, China

\* Correspondence: cchen@hbut.edu.cn

**Abstract:** Lithium-sulfur batteries with high theoretical specific capacity and high energy density are considered to be one of the most promising energy storage devices. However, the “shuttle effect” caused by the soluble polysulfide intermediates migrating back and forth between the positive and negative electrodes significantly reduces the active substance content of the battery and hinders the commercial applications of lithium–sulfur batteries. The separator being far from the electrochemical reaction interface and in close contact with the electrode poses an important barrier to polysulfide shuttle. Therefore, the electrochemical performance including coulombic efficiency and cycle stability of lithium–sulfur batteries can be effectively improved by rationally designing the separator. In this paper, the research progress of the modification of lithium–sulfur battery separators is reviewed from the perspectives of adsorption effect, electrostatic effect, and steric hindrance effect, and a novel modification of the lithium–sulfur battery separator is prospected.

**Keywords:** lithium–sulfur batteries; polysulfide; “shuttle effect”; separator; modification



**Citation:** Zhang, B.-W.; Sun, B.; Fu, P.; Liu, F.; Zhu, C.; Xu, B.-M.; Pan, Y.; Chen, C. A Review of the Application of Modified Separators in Inhibiting the “shuttle effect” of Lithium–Sulfur Batteries. *Membranes* **2022**, *12*, 790. <https://doi.org/10.3390/membranes12080790>

Academic Editor: Rahul Singh

Received: 23 July 2022

Accepted: 10 August 2022

Published: 17 August 2022

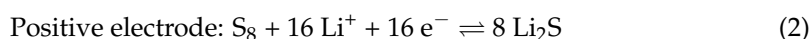
**Publisher’s Note:** MDPI stays neutral with regard to jurisdictional claims in published maps and institutional affiliations.



**Copyright:** © 2022 by the authors. Licensee MDPI, Basel, Switzerland. This article is an open access article distributed under the terms and conditions of the Creative Commons Attribution (CC BY) license (<https://creativecommons.org/licenses/by/4.0/>).

## 1. Introduction

Along with the development of mobile electronics and electric vehicles, a trend to develop energy storage devices with high efficiency and high specific energy has emerged [1–3]. Rechargeable batteries with long service life and high energy storage efficiency are attracting much attention from researchers. Among them, lithium–sulfur batteries (LSBs) have high theoretical specific capacity (1675 mAh g<sup>−1</sup>) and high energy density (2600 Wh kg<sup>−1</sup>) [4,5], and the cathode sulfur is low cost, abundant, and environmentally friendly. Therefore, LSBs have great development prospects [6]. The charge–discharge process of LSBs is a dissolution–deposition reaction [7]. During the discharge process, the cathode sulfur (S<sub>8</sub>) is electrochemically reduced to soluble long-chain lithium polysulfide Li<sub>2</sub>S<sub>x</sub> (4 ≤ x ≤ 8) first, and then converted to insoluble short-chain Li<sub>2</sub>S<sub>2</sub>/Li<sub>2</sub>S. The charging reaction is the opposite of the discharging reaction. The solid Li<sub>2</sub>S<sub>2</sub>/Li<sub>2</sub>S is first converted to short-chain LiPS, which is then further oxidized to soluble long-chain Li<sub>2</sub>S<sub>x</sub> (4 ≤ x ≤ 8), and finally to solid S<sub>8</sub>. The reaction is as follows [8]:



The “shuttle effect” of LSBs is known to be an important factor limiting their practical application [9–12]. The “shuttle effect” refers to the phenomenon that Li<sub>2</sub>S<sub>x</sub> (4 ≤ x ≤ 8) produced by the positive electrode diffuses to the negative electrode during the charging and discharging process, and is reduced to solid Li<sub>2</sub>S<sub>2</sub>/Li<sub>2</sub>S on the negative electrode surface and attached to the negative electrode. It can cause irreversible loss of battery active material, increase battery internal resistance, and decrease the theoretical capacity of LSBs [13–15].

At present, researchers have proposed many methods to suppress the “shuttle effect” of LSBs, such as electrode modification, electrolyte optimization, and separator modification. Among them, the separator is far away from the electrochemical reaction interface and in close contact with the electrode, and more importantly, it is also the diffusion channel of polysulfides (LiPSs). Therefore, its structure and performance greatly affect the electrode reaction of LSBs and the shuttle of LiPSs between the two electrodes. However, currently, the most commercialized and widely used polyolefin separators (such as polyethylene (PE) and polypropylene (PP)) have large pore sizes and do not interact with LiPSs, so they cannot inhibit the shuttle of LiPSs between the two electrodes of LSBs [16,17]. Therefore, under the premise of ensuring the basic functions of the polyolefin-based separator, if it is modified to have the function of adsorbing and/or converting LiPSs, it will be able to inhibit the “shuttle effect” of LiPSs. [18–20]. From what is known in the literature [21–24], the current separator modifications of LSBs are mainly based on confining LiPSs to the cathode region of the battery during their migration to the anode. This can be done from three perspectives: (1) modification by adsorption effect, making the separator adsorbable and fixing LiPSs on the positive side; (2) modification by electrostatic effect, making the separator repulsive and inhibiting the migration of LiPSs; (3) modification by positioning barrier effect, reducing the pore size of the separator and keeping the LiPSs in the positive electrode region by means of physical barrier. These three methods are described below.

## 2. Adsorption Effect Modification

### 2.1. Physical/Chemical Adsorption

The modification of the separator of LSBs by means of the physical adsorption effect generally refers to the use of the van der Waals force between LiPSs and the trapping material to capture LiPSs. Separator materials with high porosity and large specific surface area can provide more trapping sites, which are beneficial to inhibit the migration of LiPSs between the electrodes [25]. Therefore, attaching porous carbon materials such as carbon nanofibers, carbon flakes, microporous carbon nanofibers, reduced graphene oxide, etc. as a coating to the separator has been widely used in the separator modification of LSBs. The modification effects of different carbon materials are shown in Table 1. Generally speaking, the high sulfur loading of the cathode will increase more LiPSs in the electrolyte and result in a severer shuttle effect of LSBs. From Table 1, it can be seen that the improvement of using light mesoporous carbon as the coating to modify the separator is the most significant. At the high sulfur loading ( $3.5 \text{ mg cm}^{-2}$ ), the LSBs with this separator have a mass specific capacity of  $1021 \text{ mAh g}^{-1}$  after 100 cycles at 0.5 C, with a capacity decay rate of only 0.081%. This may be because the large number of mesopores (12 nm) in the mesoporous carbon can tune the huge volume change of  $\text{S}_8$  during the lithiation process, thereby suppressing the loss of polysulfides, which in turn controls the shuttle of LiPSs and improves the electrochemical performance of LSBs.

**Table 1.** The properties of PP separators modified with different carbon materials in LSBs.

Materials	Total Pore Volume/cm <sup>3</sup> g <sup>-1</sup>	Surface Area/m <sup>2</sup> g <sup>-1</sup>	Coating Binder Content	Area Density /mg cm <sup>-2</sup>	Cathode Sulfur Content/wt%	S Loading/mg cm <sup>-2</sup>	Capacity/(mAh g <sup>-1</sup> ) (Rate)	Cycling Performance/(mAh g <sup>-1</sup> ) (Cycles, Rate)	Capacity Decay/%	Ref.
Super P	-	-	None	0.2	55	1.1–1.3	1289 (0.5 C)	828 (200/0.2 C)	0.19	[26]
MWCNTs	2.76	410.42	None	0.17	55	-	1107 (0.5 C)	881 (150/0.2 C)	0.14	[27]
PG	3.361	1443	20 wt% PVP	0.54	63	1.8–2.0	1165 (0.5 C)	877 (150/0.5 C)	-	[28]
PC/MWCNT	0.17	83.4	10 wt% PVDF	0.51	70	1.6–1.7	911 (0.5 C)	659 (200/0.5 C)	0.138	[29]
GCFF	-	-	None	-	60	0.7	1280.14 (0.2 C)	1004.62 (100/0.2 C)	-	[30]
CFs	-	-	None	0.16	60	1	1280.14 (0.2 C)	683 (500/0.5 C)	0.071	[31]
rGO/CB	2.334	861.12	None	-	-	-	1014.5 (0.2 C)	850.9 (100/0.2 C)	0.17	[32]
CNT/AC	0.19	1312	20 wt% PVDF	-	70	-	1495.6 (0.2 C)	742 (200/0.2 C)	0.25	[33]
HCNF/rGO	-	-	None	1.2	60	1.4	1318.4 (0.2 C)	779.1(100/1 C)	0.13	[34]
mesoC	2.9	843	5 wt% super P and 10 wt% PVDF-HFP	0.5	70	3.5	1378 (0.2 C)	1021 (100/0.5 C)	0.081	[35]

Besides carbon materials, non-carbon materials can also be used as coatings to enhance the adsorption capacity of the separators of LiPSs. Deng et al. [16] prepared a polymetaphenylene isophthalamide (PMIN) separator by electrospinning. The addition of tetrabutylammonium chloride to the spinning solution produces a separator with high porosity. Using the dendritic nanofiber separator with good physical trapping effect, the LSBs exhibited a capacity decay rate of only 0.049% after 800 cycles at 0.5 C.

Chiu et al. [36] modified the PP separator of LSBs with a mixture of ethylene oxide (PEO) and lithium bis(trifluoromethanesulfonyl)imide (LiTFSI) as a coating. The experimental results show that the lithium-ion diffusion coefficient ( $9.6 \times 10^{-9} \sim 3.0 \times 10^{-8} \text{ cm}^2 \text{ s}^{-1}$ ) of PEO/LiTFSI coating is significantly higher than that of pure PP separator ( $7.6 \times 10^{-9} \sim 2.2 \times 10^{-8} \text{ cm}^2 \text{ s}^{-1}$ ). The LSBs with PEO/LiTFSI separator achieve an initial discharge capacity of  $1212 \text{ mAh g}^{-1}$  at 0.1 C and can still maintain a high reversible capacity of  $534 \text{ mAh g}^{-1}$  and a stable coulombic capacity after 200 cycles. This may be due to the fact that PEO can inhibit the diffusion of LiPSs as a gel polymer electrolyte, and the addition of LiTFSI salt enhances the ability of the lithium ion transfer of the PEO coating. The electrochemical efficiency and the synergistic effect of the PEO/LiTFSI coating are shown in Figure 1.

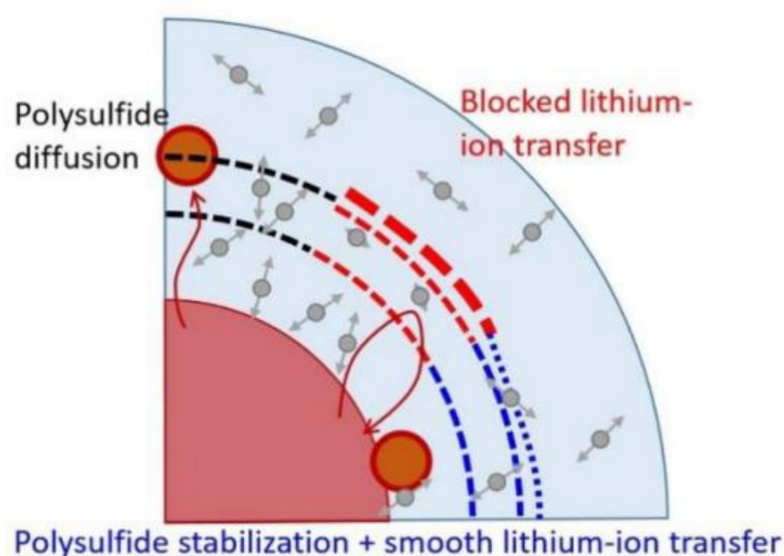


**Figure 1.** Schematic diagram of PEO/LiTFSI coating hindering LiPSs [36].

Although the modification of polyolefin separators with carbon materials can inhibit the shuttle of LiPSs between the two electrodes of LSBs to a certain extent, the interaction force between non-polar carbon materials and polar LiPSs is weak. Therefore, inhibiting the diffusion of LiPSs in the LSBs only by physical adsorption is not satisfied [37]. Compared with physical adsorption, chemical adsorption, which relies on the formation of chemical bonding forces between LiPSs and the surface atoms of adsorbent materials, can make a higher selectivity and achieve a better immobilizing effect of LiPSs [38]. For example, doping electronegative heteroatoms (such as N, O, and S, etc.) in carbon coatings can help trap LiPSs by the formation of Li–X bonds (dipole–dipole interactions) between heteroatoms and LiPSs [39,40]. Hou et al. [41] analyzed the ability of various atomically doped graphene nanoribbons (GNRs) to adsorb sulfur and  $\text{Li}_2\text{S}_x$  by density functional theory (DFT). It was found that the adsorption effect of N and O (binding energy  $-2.53 \sim -2.56 \text{ eV}$ )-doped GNRs on  $\text{Li}_2\text{S}_4$  is much greater than that of B, F, S, P, and Cl (binding energy  $-1.93 \text{ eV}$ ), which is due to the existence of dipole–dipole electrostatic interactions ( $\sim 1.95 \text{ eV}$ ). The relationship between element electronegativity and binding energy is shown in Figure 2.

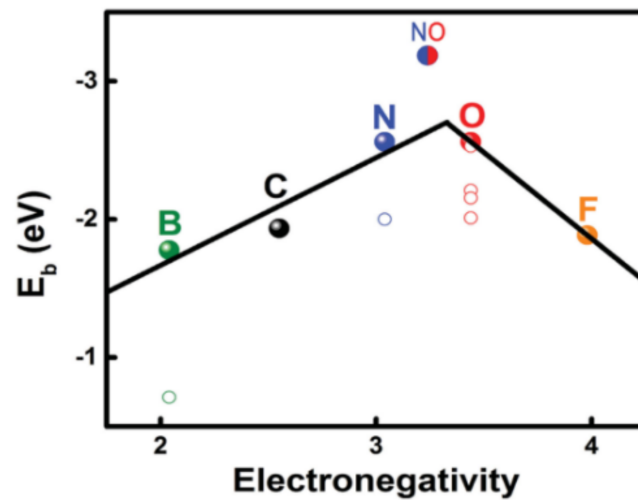


**Figure 2.** The relationship between the binding energy ( $E_b$ ) of the doping element– $\text{Li}_2\text{S}_4$  and the electronegativity of the element [41].

Zeng et al. [42] designed a honeycomb-like N, P diatomic doped carbon (HNPC) modified separator, in which the HNPC coating can effectively anchor the LiPSs by forming N–Li and P–S bonds. When using the acetylene black-sulfur composite as the cathode with the sulfur content of 79.7%, the LSBs showed excellent long-cycle stability with a capacity decay rate of only 0.06% per cycle after 900 cycles at 1 C. Figure 3 shows the cycle performance of separators modified by different coatings. It can be seen that the chemical confinement of LiPSs by diatomic doping is higher than that of single-atom doping systems.

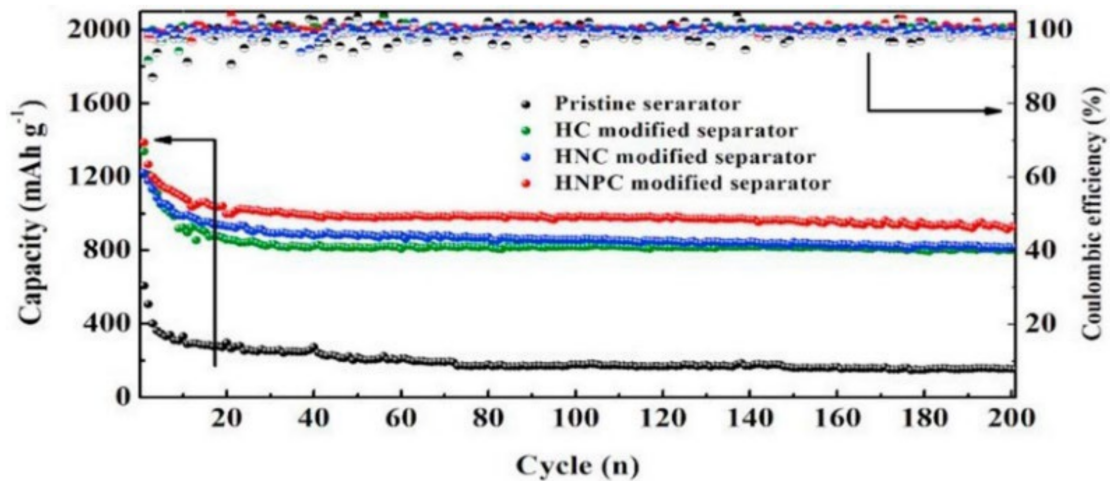


**Figure 3.** Cycle performance of LSBs using different separators at 0.2 C [42].

Besides polar atoms, the doping of polar functional groups can also realize the chemisorption of the separator to LiPSs. Pei et al. [43] used polydopamine/polyethylene oxide (PDA/PEI) to modify polyolefin separators and achieved desired results. The PDA/PEI-modified separator made the initial discharge capacity of LSBs  $1250 \text{ mAh g}^{-1}$  at 0.2 C and it remained  $900 \text{ mAh g}^{-1}$  after 100 cycles. This could be attributed to the formation of numerous C=N bonds between the amine groups in PEI and dopamine, which inhibited the accumulation of dopamine oligomers on the separator through hydrogen bonds or  $\pi$ – $\pi$  bonds, thereby making the separator hydrophilic, and the enriched N and O functional groups of the PDA/PEI coating effectively adsorbed LiPSs in the electrolyte.

In addition, the modification of PP separator with metal materials, metal oxides, and metal sulfides, the exposed metal (M) sites of which can form S–M bonds with LiPSs, are

also beneficial to improve its adsorption capacity to LiPSs [44]. Tao et al. [12] calculated by DFT that the binding energy of metal oxides and LiPSs (from  $-1.54$  to  $-7.12$  eV), is higher than that of heteroatoms and LiPSs (from  $-2.53$  to  $-2.56$  eV). Liu et al. [45] designed graphene oxide (GO) coatings doped with  $\text{TiO}_2$  nanoparticles, as shown in Figure 4a. The Ti–O–C bond formed between  $\text{TiO}_2$  and GO and the wrinkled sheet structure of GO make the combination of  $\text{TiO}_2$  and GO tight, which helps to enhance the electrical conductivity of the separator. Meanwhile, the S–Ti–O and Ti–S bonds formed between  $\text{TiO}_2$  and S enhanced the ability of the separator to adsorb LiPSs. The LSBs coated with  $\text{TiO}_2/\text{GO}$  separator can retain a reversible capacity of  $843.4 \text{ mAh g}^{-1}$  after 100 cycles at  $0.2 \text{ C}$  (Figure 4b).

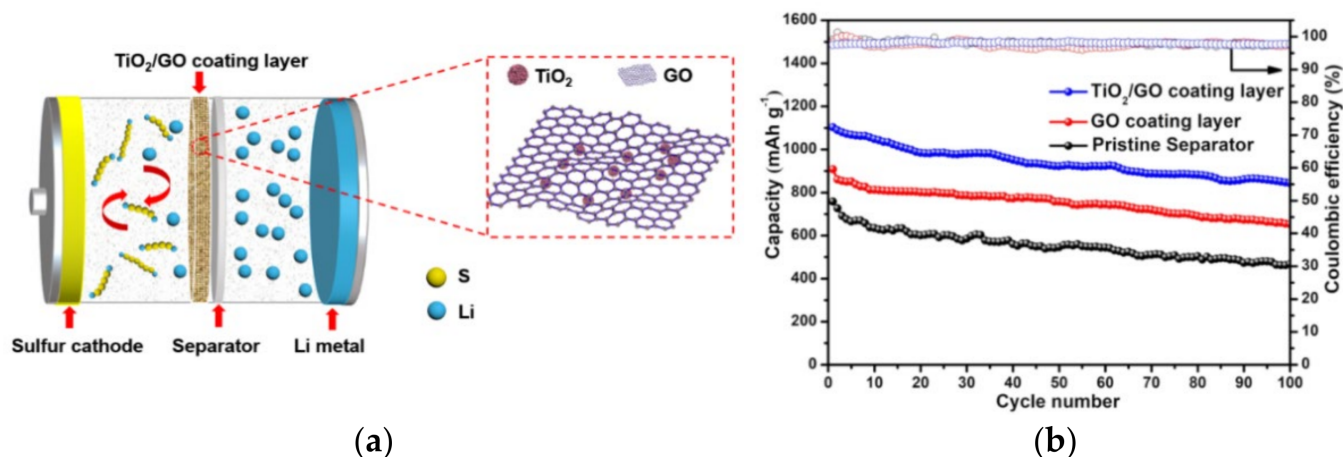


**Figure 4.** (a) Schematic diagram of LSBs with  $\text{TiO}_2/\text{GO}$  coated functional separator. (b) Cyclic performance and coulombic efficiency of the LSBs batteries with different coated separators at a rate of  $0.2 \text{ C}$  [45].

## 2.2. Catalytic Adsorption

Physical/chemical adsorption can suppress the “shuttle effect” of LiPSs, but under the conditions of high sulfur loading ( $>5 \text{ mg cm}^{-2}$ ) or long cycling, the increase of LiPSs dissolved in the electrolyte will lead to slow reaction kinetics. Moreover, the limited adsorption sites on the separator are not enough to adsorb LiPSs in the electrolyte fully, thus resulting in a low specific capacity and short cycle life of the battery. Therefore, the ability of the separator to suppress the “shuttle effect” may be reduced or even lost [46,47]. The introduction of catalytic substances on the surface of the separator can not only reduce the energy barrier of the conversion of LiPSs and insoluble  $\text{Li}_2\text{S}_2/\text{Li}_2\text{S}$ , accelerating the electrochemical reaction of LSBs, but also transfer the adsorbed LiPSs to the redox reaction in time. Thus, the content of the active substances of the battery is kept to the greatest extent, and the cycle performance of LSB is significantly improved [14].

Inherent defects in the metal oxide structure can provide more active sites for trapping and transforming LiPSs [48]. Lv et al. [49] loaded bimetallic  $\text{NiCo}_2\text{O}_4$  nanoparticles onto reduced graphene oxide as a catalytic coating for the separator. During the electrode reaction process, the oxidized metal ions ( $\text{Ni}^{3+}$  and  $\text{Co}^{3+}$ ) combine with LiPSs to form Ni–S and Co–S bonds, which anchor the LiPSs to the  $\text{NiCo}_2\text{O}_4/\text{rGO}$  surface to suppress the “shuttle effect” of LSBs. Furthermore, DFT calculations show that the  $\text{NiCo}_2\text{O}_4$  (100) crystal surface has a low Li-ion diffusion barrier ( $0.15 \text{ eV}$  compared to  $0.293 \text{ eV}$  for carbon materials), which helps to improve the migration rate of lithium ions and promote lithium-ion–electron coupling, thereby accelerating the conversion of LiPSs to  $\text{Li}_2\text{S}_2/\text{Li}_2\text{S}$ . Using a core-shell structure material (encapsulated sulfur in carbon) with a sulfur content of 70 wt% as the cathode and under the condition of a high sulfur loading of  $6 \text{ mg cm}^{-2}$ , the LSBs showed the capacity loss rate only 0.02% after 400 cycles at a current density of  $1 \text{ mA cm}^{-2}$ , and at the same time, there was an excellent areal capacity of  $7.1 \text{ mAh cm}^{-2}$ .

Adding other metals to monometallic compounds can also improve the reaction kinetics of LiPS transformation on the surface of metal compounds [50]. Zhang et al. [51] introduced Mo atoms into Ni<sub>3</sub>N and used a composite of multi-walled carbon nanotubes and Ni<sub>0.2</sub>Mo<sub>0.8</sub>N to modify the separator. During the electrochemical reaction process, the Mo atoms in the Ni<sub>0.2</sub>Mo<sub>0.8</sub>N are etched and leached out by LiPSs, leaving a large number of vacancies around Ni (Figure 5a). The vacancies formed can accelerate the charge transfer and the LiPS conversion. The potential of the Ni<sub>3</sub>N and Mo<sub>2</sub>N surfaces in the coating is higher than lithium negative electrode, thus creating an electric field between the separator and the lithium anode (Figure 5b), which promotes the directional movement of sulfur and lithium ions and inhibits the shuttling of LiPSs to some extent. The LSBs with this separator can achieve an initial battery capacity of 1097.2 mAh g<sup>-1</sup> at a high rate of 5 C.

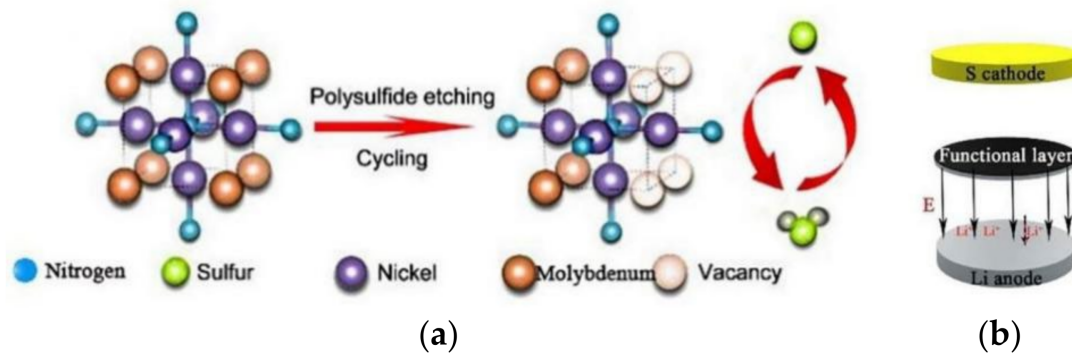


Figure 5. (a) Mechanism of in-situ etching of LiPSs by bimetallic nitride. (b) Direction of the electric field inside the LSBs [51].

Due to the abundant pore structures and catalytic sites, metal–organic frameworks (MOFs) composed of organic ligands and transition metal ions have been widely used for catalytic modification of the separators of LBSs. The pore structure in MOFs can promote the adequate contact between the separator and the electrolyte and limits the diffusion of LiPSs, while the metal central ions can chemisorb and catalyze LiPSs [41]. Hong et al. [52] doped cerium-based metal-organic frameworks (Ce-MOFs) into CNTs to form Ce-MOFs/CNT separator coatings. The large specific surface area of Ce-MOFs and the ligated unsaturated Ce (IV) cluster nodes can rapidly adsorb LiPSs and accelerate the conversion between LiPSs and Li<sub>2</sub>S<sub>2</sub>/Li<sub>2</sub>S, which is shown in Figure 6a. As seen, under the high sulfur loading of 6 mg cm<sup>-2</sup>, the initial specific capacity of LSBs was 1021.8 mAh g<sup>-1</sup> at 1 C, which slowly decreased to 838.8 mAh g<sup>-1</sup> after 800 cycles with a decay rate of only 0.022% per cycle, as shown in Figure 6b. The coulombic efficiency of the LSBs was close to 100%, which suggesting its excellent cycle performance.

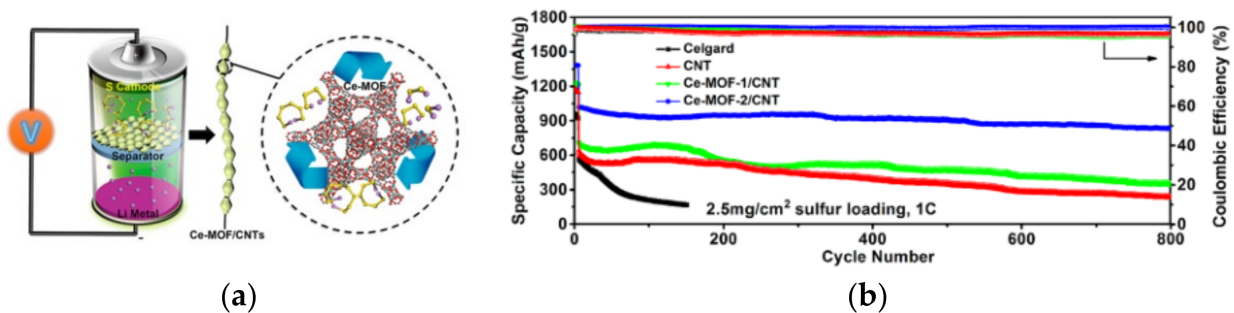
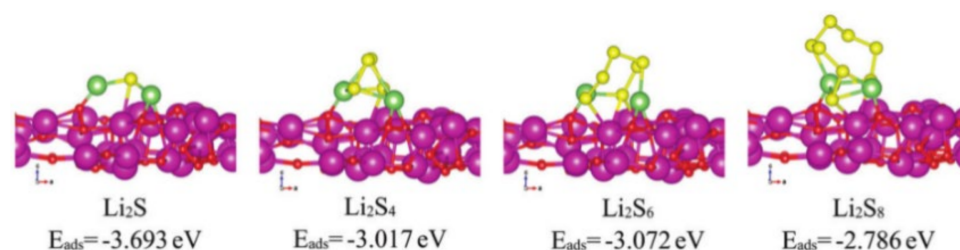


Figure 6. (a) Schematic representation of the catalytic conversion of LiPSs on the surface of Ce-MOFs/CNT separators. (b) Cyclic performance of cells with different separator at 1 C for 800 cycles (2.5 mg/cm<sup>2</sup> sulfur loading) [52].

In addition to transition metal elements, rare-earth elements have also been used in the catalytic modification of the separators of LBSs. Peng et al. [53] prepared a novel pp separator coated with  $\text{Eu}_2\text{O}_3$ /Ketjen black ( $\text{Eu}_2\text{O}_3$ /KB). The exposed (222) plane of  $\text{Eu}_2\text{O}_3$  exhibits strong polarity-polarity interaction with LiPSs, which is beneficial to confine the transfer of LiPSs. The adsorption energy of  $\text{Eu}_2\text{O}_3$  with LiPSs is shown in Figure 7. Apart from that, oxygen vacancies in  $\text{Eu}_2\text{O}_3$  can provide more catalytic sites for regulating  $\text{Li}_2\text{S}$  precipitation. Therefore, with high crystal face index,  $\text{Eu}_2\text{O}_3$  can lower the energy barrier for  $\text{Li}_2\text{S}$  nucleation on it and promote the conversion of LiPSs to  $\text{Li}_2\text{S}$ . The LBSs with  $\text{Eu}_2\text{O}_3$ /KB modified separator exhibited excellent cycling stability and rate capability. Its capacity decay rate achieved only 0.05% per cycle during 500 cycles at 1 C.



**Figure 7.** Adsorption energies of different LiPSs on the  $\text{Eu}_2\text{O}_3$  (222) plane [53].

Some non-metallic materials with catalytic activity have also been used in the separator of LBSs to promote the conversion of LiPSs. For example, Wang et al. [54] used red phosphorus (RP) as a coating to enhance the sulfur reaction kinetics of LSBs. Through Lewis acid–base interaction, The  $\text{Li}_3\text{PO}_4$  with high conductivity was formed by RP and LiPSs, which can improve the conductivity of lithium ions and promote the redox reaction of sulfur. However, the formation of  $\text{Li}_3\text{PO}_4$  consumes some active sites for adsorbing LiPSs in the separator, which may lead to the decrease of the capacity of the LSBs under long-term cycling. The LSBs with RP-modified separator exhibited a capacity of  $729.6 \text{ mAh g}^{-1}$  after 500 cycles at 1 C with a capacity retention rate of 82%.

### 3. Electrostatic Effect

The sulfur atoms at the end of LiPSs possess a large number of negative charges and free radicals. The introduction of negatively charged species on the separator can inhibit the shuttle of polysulfide ions through electrostatic repulsion and simultaneously facilitate  $\text{Li}^+$  migration. This could decrease the resistance between the positive electrode and the separator, preventing the energy generated by the battery from dissipating in the form of thermal energy [39,55].

#### 3.1. Negatively Charged Group

Song et al. [56] grafted polyacrylic acid (PAA) on the surface of PP separator (PP-g-PAA). A large number of carboxyl functional groups in PAA can not only repel LiPSs anions through electrostatic interaction, but also enhance the hydrophilicity of the separator and reduce the internal resistance of LSBs. Chiu et al. [57] prepared a gel polymer electrolyte separator coating by mixing polymethyl methacrylate with rich -COO- and LiTFSI. When the sulfur loading of the cathode was increased from 4 to  $10 \text{ mg cm}^{-2}$ , the lithium-ion diffusion coefficient of LSBs slightly decreased from  $5.27 \times 10^{-9}$ – $3.1 \times 10^{-8} \text{ cm}^2 \text{ s}^{-1}$  to  $2.09 \times 10^{-9}$ – $1.27 \times 10^{-8} \text{ cm}^2 \text{ s}^{-1}$ , which indicates that the coating enhances the lithium-ion transfer efficiency and suppresses the diffusion of LiPSs. Under the high sulfur loading of  $8 \text{ mg cm}^{-2}$ , LSBs with this separator exhibit a high area capacity of  $7.1 \text{ mWh cm}^{-2}$ . Li et al. [58] modified PP with  $\text{Fe}_3\text{O}_4$  nanoparticles and carboxylated carbon nanotubes (CTs-COOH). The  $\text{Fe}_3\text{O}_4$  layer acts as an “upper current collector” and facilitates electron transport, while -COOH can inhibit the transport of LiPSs through electrostatic effects. The synergistic effect of the two factors enables LSBs to have a capacity decay rate as low as 0.032% per cycle when cycled for 2000 times at 1 C.

Nafion with rich sulfonic acid groups (-SO<sub>3</sub>H) is also widely used in the modification of the separators of LSBs. But due to the poor conductivity, an overly thick coating of Nafion will reduce the lithium-ion transport capacity of the separator [59]. Zhuang et al. [60] designed a ternary-layer separator composed of PP, graphene oxide (GO) and Nafion for LSBs (Figure 8), in which the ultrathin GO layer (0.0032 mg cm<sup>-2</sup>, about 40 layers) can cover the macropores of the PP matrix and provides support for the Nafion layer. The Nafion layer with the areal loading of 0.05 mg cm<sup>-2</sup> also retains the conductivity of the separator while repelling LiPSs. The specific capacity of LSBs using the ternary layer separator can reach a discharge capacity of 1057 mAh g<sup>-1</sup> at 0.1 C.

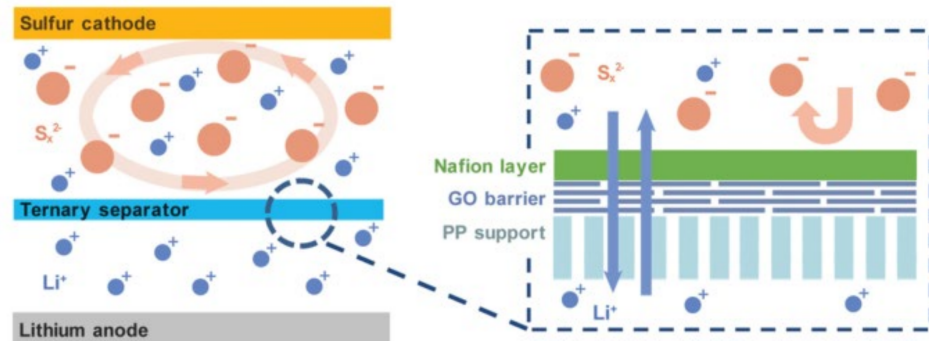


Figure 8. Schematic diagram of ternary PP/GO/Nafion separator [60].

In addition, the confinement of LiPSs can also be achieved by using the charge environment between the two-dimensional material layers. Xu et al. [61] used two-dimensional vermiculite nanosheets to prepare the separators of LSBs, the structure of which is shown in Figure 9. The vermiculite nanosheet is negatively charged, so the positively charged lithium ions can be transferred between the layers, while the negatively charged polysulfide ions cannot diffuse due to electrostatic interaction. This effectively suppressed the transmembrane diffusion of LiPSs.

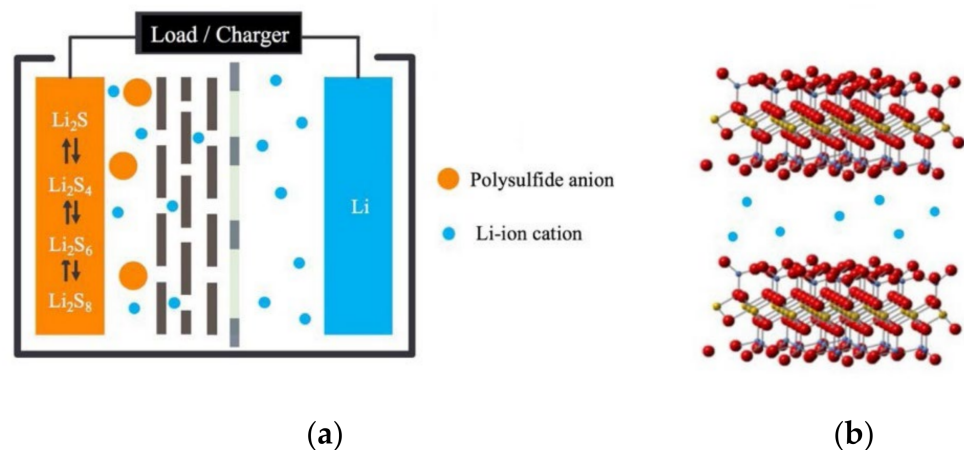
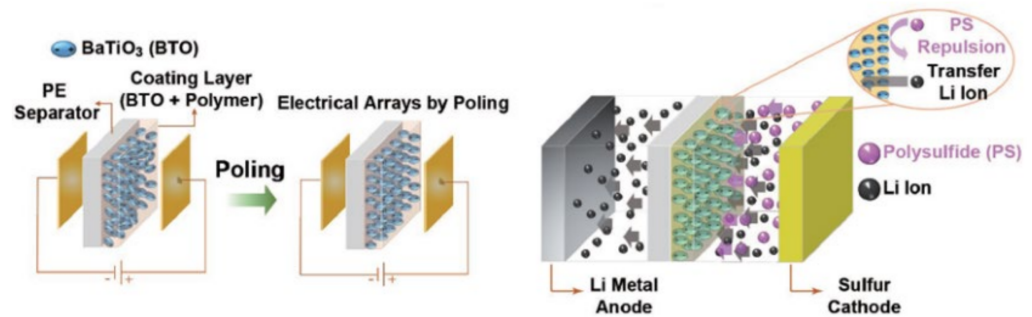


Figure 9. (a) Schematic diagram of LSBs sheet vermiculite separator, (b) vermiculite sheet structure [61].

### 3.2. Polar Particles

Besides negatively charged groups, some polar particles can also repel LiPSs through electrostatic effects. BaTiO<sub>3</sub> (BTO) with high dielectric constant can generate a large number of positive and negative charges on the surface of BTO through spontaneous polarization, which can electrostatically interact with lithium ions and polar molecules LiPSs [62]. Yim et al. [63] embedded BTO particles into PE separators. The polar BTO forms permanent dipoles under the action of electric field (Figure 10), which can block LiPSs through electrostatic repulsion, thereby improving the cycling performance of LSBs. The polarized

BTO coating can also enhance the mechanical stability of the PE separator and improve the capacity and cycle life of the LSBs. At a current density of 0.5 C, the LSBs with this separator applied achieves an initial discharge capacity of  $1122.1 \text{ mAh g}^{-1}$ .



**Figure 10.** Schematic diagram of the polarization process of BTO/PE and the repulsive effect of polarized BTO on LiPSs [63].

#### 4. Steric Hindrance Effect

The pore size of commonly used polyolefin separators (about 100 nm) is much larger than the size of LiPSs, which cannot block the shuttle of LiPSs between the cathode and anode of LSBs. Thus, reducing the pore size of the diaphragm can hinder the diffusion of LiPSs to the anode [64]. The modification methods of LSBs separators based on this steric hindrance effect can be broadly classified into two categories: (1) accumulation of particles on the surface of the separator to form a densely modified layer covering the original macropores; (2) construction of a new microporous separator using microporous materials.

##### 4.1. Particle Buildup

Maletti et al. [65] prepared a lithium vanadium oxide ( $\text{LiV}_3\text{O}_8$ )-coated separator. The dense coating formed by  $\text{LiV}_3\text{O}_8$  nanoparticles can cover the original macropore structure of the PP separator, forming a physical barrier to inhibit the diffusion of LiPSs.  $\text{LiV}_3\text{O}_8$  can disproportionate with LiPSs to promote the conversion of LiPSs to  $\text{Li}_2\text{S}_2/\text{Li}_2\text{S}$  (Figure 11). In addition, the  $\text{LiV}_3\text{O}_8$  coating significantly reduces the resistance of the cell by facilitating charge transfer at the cathode/diaphragm coating interface. Compared with pure PP, the charge transfer resistance of LSBs with  $\text{LiV}_3\text{O}_8$  separator was significantly reduced by 83%, with a high initial discharge capacity of  $1254 \text{ mAh g}^{-1}$  at a current density of 0.2 C and a capacity decay rate of 0.063% after 500 cycles at 0.5 C.

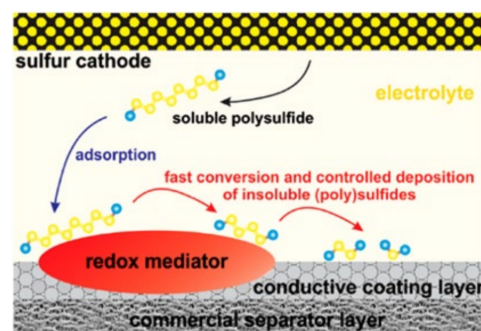


**Figure 11.** Schematic representation of the adsorption and redox transformation of LiPSs at the  $\text{LiV}_3\text{O}_8$  diaphragm interface [65].

Besides the pore size reduction that is possible by loading zero-dimensional nanoparticles on the surface of the separator, the layered structure formed by the stacking of two-dimensional nanosheets can also form a physical barrier to intercept LiPSs. Ghazi et al. [66] deposited multilayer  $\text{MoS}_2$  nanosheets with a thickness of about 350 nm on the surface of

polyolefin separators. The formed dense structure can effectively block LiPSs, and at the same time, the voids between the MoS<sub>2</sub> nanosheets can prevent solid LiS from forming an insulating layer on the separator and provide a transfer channel for lithium ions, which realizes the effective sieving of LiPSs and lithium ions.

Chang et al. [67] designed a two-dimensional MOF sheet molecular sieve (CuBDCs) coating with one-dimensional vertical channels. The structure is shown in Figure 12. The one-dimensional channels (about 5.2 Å) in the CuBDCs nanosheets are much smaller than the size of polysulfides, which can act as molecular sieves and hinder the diffusion of LiPSs to the anode. Secondly, the CuBDC sheet is approximately 10 nm thick, which combined with its internal one-dimensional channels shortens the ion transport path, improving the mobility of Li ions. The LSBs using this separator can still maintain a specific capacity of 830 mAh g<sup>-1</sup> after 1000 long cycles at 1 C. This indicates that the 2D CuBDC sheets have excellent sieving ability for LiPSs.

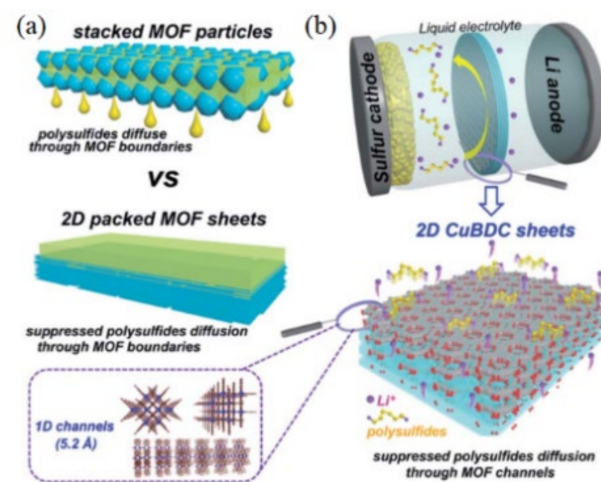


**Figure 12.** (a) Schematic illustration of granular and 2D sheet MOFs for inhibiting LiPSs; (b) schematic illustration of 2D CuBDC sheets with crystal structures of 1D nanochannels and 2D CuBDC sheets [66].

#### 4.2. New Microporous Separator

A commonly used way to reduce the pore size of polyolefin separators is to coat their surfaces with small-pore-size coatings, and carbon coatings with nanopores have been shown to have good performance in inhibiting the “shuttle effect” of LiPSs under high sulfur-loading conditions [68]. However, the surface energy of the polyolefin separator is low, and it is difficult to adhere a uniform coating material on the surface of the separator. Therefore, the phenomenon of the coating peeling off the separator during the cycle occurs occasionally. Using novel functional separators as substrates is one of the fundamental solutions to this problem.

Compared with the traditional polyolefin separator, the electrospun nanofiber separator has higher porosity and chemical stability. The strong affinity of electrospun nanofibers for the electrolyte can significantly improve the mobility of lithium ions in LSBs, thereby effectively inhibiting the “shuttle effect” of LSBs [69]. Pei et al. [70] prepared a structurally asymmetric aramid nanofiber Janus separator (ANF-JS). The separator structure is shown in Figure 13. The side of the separator facing the positive electrode is a nanoporous layer with ion selectivity, which can hinder the shuttling of LiPSs between electrodes; the side of the separator facing the negative electrode is a microporous layer with a three-dimensional porous structure, which can provide channel for electrolyte absorption and fast lithium-ion transport. After 1000 cycles at 1 C with this separator, the capacity decay rate of the LSBs is reduced to 0.0195% per cycle.

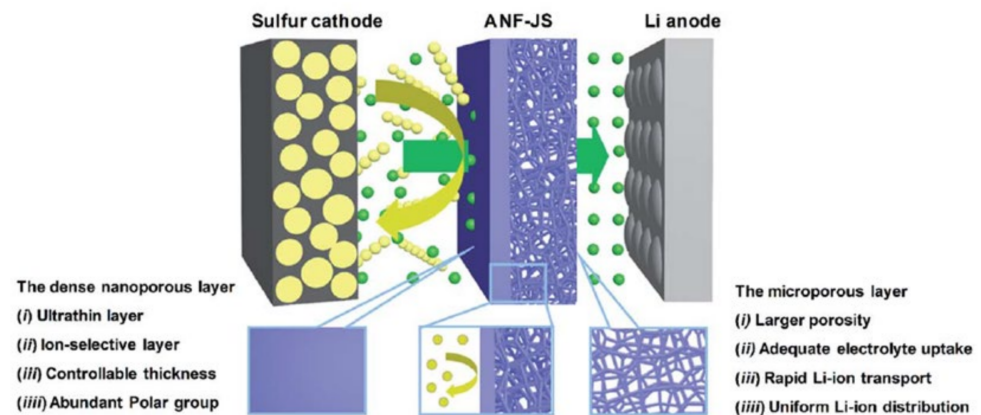


**Figure 13.** Schematic illustration of ANF-JS applied to LiPSs and Li-ion transport in LSBs [70].

Doping functional particles in the novel separator can combine the steric hindrance effect with other effects, enabling the separator to further inhibit the shuttle of LiPSs [71]. Guo et al. [72] prepared a flexible  $\text{Ti}_4\text{O}_7/\text{C}$  nanofiber barrier layer (TCNFs) by electrospinning. Figure 14a shows the adsorption–desorption and BET curves, and it can be seen that the pore size of the separator was between 2 and 16 nm and the specific surface area was  $40 \text{ m}^2 \text{ g}^{-1}$ , which can effectively isolate LiPSs from the positive side of LSBs. The TCNFs separator has dual effects of physical shielding and chemical adsorption on LiPSs, which make the capacity fade of the LSBs only 0.03% per cycle after 2500 cycles, even at a current density of 3 C, as shown in Figure 14b.

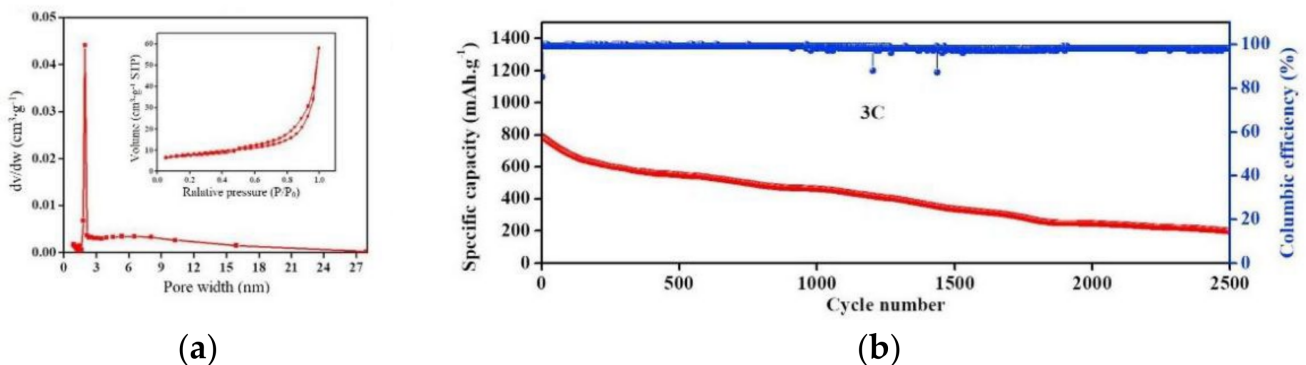


**Figure 14.** (a) Pore size distribution and  $\text{N}_2$  adsorption–desorption isotherms of TCNFs; (b) cycling performance of CMK3–S/TCNFs at high current density 3 C [72].

Wang et al. [73] prepared separators (ZIF-7@PCF) with cross-linked structures by growing two-dimensional MOF sheets (ZIF-7) on porous carbon nanofibers (PCFs), as shown in Figure 15a. The pores of the separator are mostly mesopores and micropores with diameters of less than 10 nm, which are beneficial to hinder the transport of LiPSs. PCF porous carbonaceous framework can facilitate electron and ion transport in batteries, while ZIF-7 MOF provides an abundant active site for the capture and conversion of LiPS. Under high sulfur-loading conditions of  $6 \text{ mg cm}^{-2}$ , the LSB with ZIF-7@PCF exhibits an initial discharge specific capacity of  $1221 \text{ mAh g}^{-1}$  at a current density of 0.2 C and a discharge specific capacity of  $661.3 \text{ mAh g}^{-1}$  at 5 C, showing good rate performance, as shown in Figure 15b.

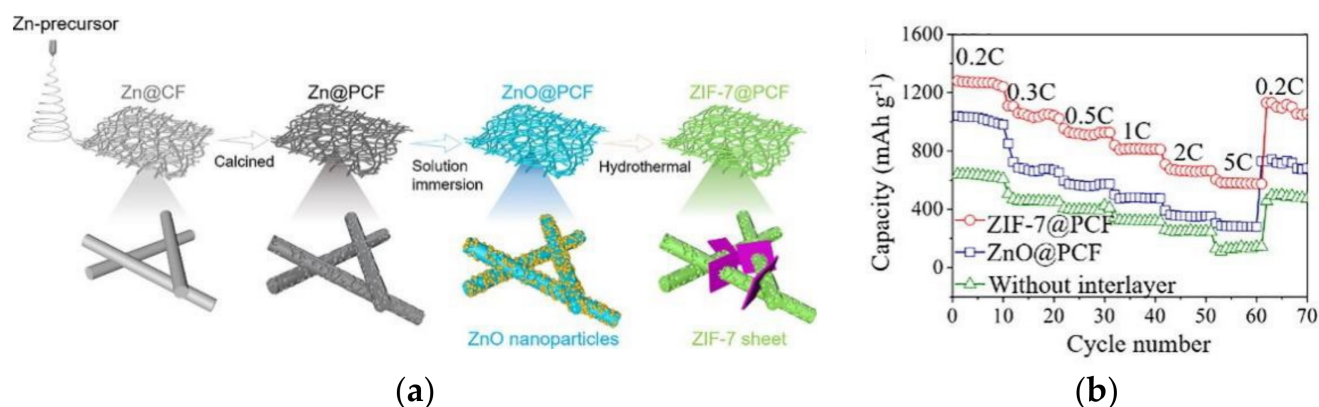


**Figure 15.** (a) Schematic diagram of preparation process of ZIF-7@PCF interlayer; (b) the rate capability of cells with ZIF-7@PCF, ZnO@PCF interlayer, and without interlayer [73].

## 5. Conclusions

This paper mainly introduces the methods of modifying the lithium–sulfur battery separators by the adsorption effect, electrostatic effect, and steric hindrance effect using polyolefin separator as the matrix. Compared with the traditional polyolefin separator, the modified separators have good function for inhibiting the “shuttle effect” of LiPSs. Especially, the modified separator with catalytic effect can maximize the utilization of the active species in LSBs, showing excellent cycling and rate performance under long-cycle conditions and high sulfur loading. The current separator modification materials for high sulfur loading and low electrolyte LSBs are mainly carbon-based composites with hollow or layered structures, and the robust internal porous network structure can provide buffers for sulfur volume changes and the shuttle of LiPSs. However, overly thick carbon coating will reduce the actual energy density of the battery, so lightweight materials such as graphene can be selected as the base layer to reduce the thickness of the coating and the load quality. To realize the high energy density and rate capability of LSBs, it is possible to consider using nanoscale catalytic materials with large specific surface area and short ion transport distance or gel electrolyte materials with high ionic conductivity to modify the separator. In addition, the functional modification of novel nanofiber separators with high chemical stability and electrolyte affinity also opens up new avenues for developing high-energy-density LSB separators.

**Author Contributions:** Conceptualization, C.C., Y.P. and B.-M.X.; writing—original draft preparation, B.-W.Z.; writing—review and editing, B.-W.Z.; article revision, B.S.; literature review, P.F.; illustrations and tables, F.L. and C.Z.; visualization, C.C.; supervision, Y.P. and B.-M.X.; funding acquisition, C.C. All authors have read and agreed to the published version of the manuscript.

**Funding:** This work was supported by the Doctoral Scientific Research Foundation of Hubei University of Technology (Grant No. BSQD2019030).

**Institutional Review Board Statement:** Not applicable.

**Informed Consent Statement:** Not applicable.

**Data Availability Statement:** Data sharing not applicable.

**Acknowledgments:** The authors are thankful to School of Materials and Chemical Engineering, Hubei University of Technology, China.

**Conflicts of Interest:** The authors declare no conflict of interest.

## References

1. Islam, M.S.; Nazar, L.F. Advanced materials for lithium batteries. *J. Mater. Chem.* **2011**, *21*, 9810. [[CrossRef](#)]
2. Ma, Y.; Xie, X.B.; Yang, W.Y.; Yu, Z.P.; Sun, X.Q.; Zhang, Y.P.; Yang, X.Y.; Kimura, H.; Hou, C.X.; Guo, Z.H.; et al. Recent advances in transition metal oxides with different dimensions as electrodes for high-performance supercapacitors. *Adv. Compos. Hybrid Mater.* **2021**, *4*, 906–924. [[CrossRef](#)]
3. Zhai, I.Y.; Yang, W.; Xie, X.; Yu, Z.P.; Sun, X.Q.; Zhang, Y.P.; Yang, X.Y.; Kimura, H.; Hou, C.X.; Guo, Z.H.; et al. Co<sub>3</sub>O<sub>4</sub> nanoparticle-dotted hierarchical-assembled carbon nanosheet framework catalysts with the formation/decomposition mechanisms of Li<sub>2</sub>O<sub>2</sub> for smart lithium–oxygen batteries. *Inorg. Chem. Front.* **2022**, *9*, 1115–1124. [[CrossRef](#)]
4. Ould, E.T.; Kamzabek, D.; Chakraborty, D.; Doherty, M.F. Lithium–sulfur batteries: State of the art and future directions. *ACS Appl. Energy Mater.* **2018**, *1*, 1783–1814. [[CrossRef](#)]
5. Chen, H.; Wang, C.; Dong, W.; Lu, W.; Du, Z.L.; Chen, L.W. Monodispersed sulfur nanoparticles for lithium–sulfur batteries with theoretical performance. *Nano Lett.* **2015**, *15*, 798–802. [[CrossRef](#)] [[PubMed](#)]
6. Zhao, M.; Li, B.Q.; Zhang, X.Q.; Huang, J.Q.; Zhang, Q. A perspective toward practical lithium–sulfur batteries. *ACS Cent. Sci.* **2020**, *6*, 1095–1104. [[CrossRef](#)] [[PubMed](#)]
7. Li, G.; Wang, S.; Zhang, Y.; Li, M.; Chen, Z.W.; Lu, J. Revisiting the role of polysulfides in lithium–sulfur batteries. *Adv. Mater.* **2018**, *30*, 1705590. [[CrossRef](#)] [[PubMed](#)]
8. Abbas, S.A.; Ding, J.; Wu, S.H.; Fang, J.; Boopathi, K.M.; Mohapatra, A.; Lee, L.W.; Wang, P.C.; Chang, C.C.; Chu, C.W. Modified separator performing dual physical/chemical roles to inhibit polysulfide shuttle resulting in ultrastable Li–S batteries. *ACS Nano* **2017**, *11*, 12436–12445. [[CrossRef](#)]
9. He, Y.; Qiao, Y.; Chang, Z.; Cao, X.; Jia, M.; He, P.; Zhou, H. Developing A “Polysulfide-Phobic” Strategy to Restrain Shuttle Effect in Lithium-Sulfur Batteries. *Angew. Chem.* **2019**, *58*, 11774–11778. [[CrossRef](#)]
10. Yan, J.; Liu, X.; Li, B. Capacity Fade Analysis of Sulfur Cathodes in Lithium-Sulfur Batteries. *Adv. Sci.* **2016**, *3*, 1600101–1600111. [[CrossRef](#)]
11. Li, T.; Bai, X.; Gulzar, U.; Bai, Y.J.; Capiglia, C.; Deng, W.; Zhou, X.F.; Liu, Z.P.; Feng, Z.F.; Zaccaria, R.P. A Comprehensive Understanding of Lithium–Sulfur Battery Technology. *Adv. Funct. Mater.* **2019**, *29*, 1901730. [[CrossRef](#)]
12. Tao, X.; Wang, J.; Liu, C.; Wang, H.; Yao, H.; Zheng, G.Y.; Seh, Z.W.; Cai, Q.X.; Li, W.Y.; Zhou, G.; et al. Balancing surface adsorption and diffusion of lithium-polysulfides on nonconductive oxides for lithium-sulfur battery design. *Nat. Commun.* **2016**, *7*, 11203. [[CrossRef](#)]
13. Manthiram, A.; Fu, Y.; Su, Y.S. Challenges and prospects of lithium–sulfur batteries. *Acc. Chem. Res.* **2013**, *46*, 1125–1134. [[CrossRef](#)]
14. Manthiram, A.; Chung, S.H.; Zu, C. Lithium–sulfur batteries: Progress and prospects. *Adv. Mater.* **2015**, *27*, 1980–2006. [[CrossRef](#)]
15. Dent, M.; Jakubczyk, E.; Zhang, T.; Lekakou, C. Kinetics of sulphur dissolution in lithium–sulphur batteries. *J. Phys. Energy* **2022**, *4*, 024001. [[CrossRef](#)]
16. Deng, N.; Wang, Y.; Yan, J.; Ju, J.; Li, Z.J.; Fan, L.L.; Zhao, H.J.; Kang, W.M.; Cheng, B.W. A F-doped tree-like nanofiber structural poly-m-phenyleneisophthalamide separator for high-performance lithium-sulfur batteries. *Power Sources* **2017**, *362*, 243–249. [[CrossRef](#)]
17. Dong, Q.; Shen, R.; Li, C.; Gan, R.Y.; Ma, X.T.; Wang, J.C.; Li, J.; Wei, Z.D. Construction of Soft Base Tongs on Separator to Grasp Polysulfides from Shuttling in Lithium-Sulfur Batteries. *Small* **2018**, *14*, 1804277. [[CrossRef](#)]
18. Liu, Y.T.; Liu, S.; Li, G.R.; Guo, X.P. Strategy of enhancing the volumetric energy density for lithium–sulfur batteries. *Adv. Mater.* **2021**, *33*, 2003955. [[CrossRef](#)]
19. Wang, P.; Xi, B.; Huang, M.; Chen, W.H.; Feng, J.K.; Xiong, S.L. Emerging catalysts to promote kinetics of lithium–sulfur batteries. *Adv. Energy Mater.* **2021**, *11*, 2002893. [[CrossRef](#)]
20. Fang, R.; Zhao, S.; Sun, Z.; Wang, D.W.; Chen, H.M.; Li, F. More reliable lithium-sulfur batteries: Status, solutions and prospects. *Adv. Mater.* **2017**, *29*, 1606823. [[CrossRef](#)]
21. Chung, S.H.; Chang, C.H.; Manthiram, A. Hierarchical sulfur electrodes as a testing platform for understanding the high-loading capability of Li-S batteries. *J. Power Sources* **2016**, *334*, 179–190. [[CrossRef](#)]
22. Dang, C.; Mu, Q.; Xie, X.; Sun, X.; Yang, X.; Zhang, Y.P.; Maganti, S.; Huang, M.; Jiang, Q.L.; Seok, I.; et al. Recent progress in cathode catalyst for nonaqueous lithium oxygen batteries: A review. *Adv. Compos. Hybrid Mater.* **2022**, *5*, 606–626. [[CrossRef](#)]
23. Zhang, K.; Chen, Z.X.; Ning, R.Q.; Xi, S.B.; Du, Y.H.; Liu, C.B.; Ren, Z.Y.; Chi, X.; Bai, M.H.; Shen, C.; et al. Single-Atom Coated Separator for Robust Lithium-Sulfur Batteries. *ACS Appl. Mater. Interfaces* **2019**, *11*, 25147–25154. [[CrossRef](#)]
24. Song, C.W.; Peng, C.X.; Bian, Z.H.; Dong, F.; Xu, H.Y.; Zheng, S.Y. Stable and Fast Lithium–Sulfur Battery Achieved by Rational Design of Multifunctional Separator. *Energy Environ. Mater.* **2019**, *2*, 216–224. [[CrossRef](#)]
25. Liao, H.Y.; Zhang, H.Y.; Hong, H.Q.; Li, Z.H.; Lin, Y.X. Novel flower-like hierarchical carbon sphere with multi-scale pores coated on PP separator for high-performance lithium-sulfur batteries. *Electrochim. Acta* **2017**, *257*, 210–216. [[CrossRef](#)]
26. Chung, S.H.; Manthiram, A. Bifunctional Separator with a Light-Weight Carbon-Coating for Dynamically and Statically Stable Lithium-Sulfur Batteries. *Adv. Funct. Mater.* **2014**, *24*, 5299–5306. [[CrossRef](#)]
27. Chung, S.H.; Manthiram, A. High-Performance Li-S Batteries with an Ultra-lightweight MWCNT-Coated Separator. *J. Phys. Chem. Lett.* **2014**, *5*, 1978–1983. [[CrossRef](#)]
28. Zhai, P.Y.; Peng, H.J.; Cheng, X.B.; Zhu, L.; Huang, J.Q.; Zhu, W.C.; Zhang, Q. Scaled-up fabrication of porous-graphene-modified separators for high-capacity lithium–sulfur batteries. *Energy Storage Mater.* **2017**, *7*, 56–63. [[CrossRef](#)]

29. Tan, L.; Li, X.H.; Wang, Z.X.; Guo, H.J.; Wang, J.X.; An, L. Multifunctional Separator with Porous Carbon/Multi-Walled Carbon Nanotube Coating for Advanced Lithium–Sulfur Batteries. *Chemelectrochem* **2018**, *5*, 71–77. [[CrossRef](#)]
30. Lee, D.K.; Ahn, C.W.; Jeon, H.J. Web-structured graphitic carbon fiber felt as an interlayer for rechargeable lithium-sulfur batteries with highly improved cycling performance. *J. Power Sources* **2017**, *360*, 559–568. [[CrossRef](#)]
31. Zhang, B.; Yu, L.; Zhao, Y. Ultralight carbon flakes modified separator as an effective polysulfide barrier for lithium-sulfur batteries. *Electrochim. Acta* **2019**, *295*, 910–917. [[CrossRef](#)]
32. Zhang, K.M.; Dai, L.Q.; Xie, L.J.; Kong, Q.Q.; Su, F.Y.; Shi, J.; Liu, Y.Z. Graphene/Carbon Black Co-modified Separator as Polysulfides Trapper for Li-S Batteries. *Chemistryselect* **2019**, *4*, 6026–6034. [[CrossRef](#)]
33. Guo, Y.F.; Xiao, J.R.; Hou, Y.X.; Wang, Z.Y.; Jiang, A.H. Carbon nanotube doped active carbon coated separator for enhanced electrochemical performance of lithium–sulfur batteries. *J. Mater. Sci. Mater. Electron.* **2017**, *28*, 17453–17460. [[CrossRef](#)]
34. Zhang, Z.A.; Wang, G.C.; Lai, Y.Q.; Li, J. A freestanding hollow carbon nanofiber/reduced graphene oxide interlayer for high-performance lithium–sulfur batteries. *J. Alloys Compd.* **2016**, *663*, 501–506. [[CrossRef](#)]
35. Balach, J.; Jaumann, T.; Klose, M.; Oswald, S.; Eckert, J.; Giebeler, L. Functional Mesoporous Carbon-Coated Separator for Long-Life, High-Energy Lithium-Sulfur Batteries. *Adv. Funct. Mater.* **2015**, *25*, 5285–5291. [[CrossRef](#)]
36. Chiu, L.L.; Chung, S.H. A Poly(ethylene oxide)/Lithium bis(trifluoromethanesulfonyl)imide-Coated Polypropylene Membrane for a High-Loading Lithium-Sulfur Battery. *Polymers* **2021**, *13*, 535. [[CrossRef](#)]
37. Fan, Y.; Niu, Z.; Zhang, F.; Zhang, R.; Zhao, Y.; Lu, G. Suppressing the Shuttle Effect in Lithium-Sulfur Batteries by a UiO-66-Modified Polypropylene Separator. *ACS Omega* **2019**, *4*, 10328–10335. [[CrossRef](#)]
38. Li, N.; Xie, Y.; Peng, S.T.; Xiong, X.; Han, K. Ultra-lightweight Ti<sub>3</sub>C<sub>2</sub>T MXene modified separator for Li–S batteries: Thickness regulation enabled polysulfide inhibition and lithium ion transportation. *J. Energy Chem.* **2020**, *42*, 116–125. [[CrossRef](#)]
39. Zuo, X.; Zhen, M.; Wang, C. Ni@N-doped graphene nanosheets and CNTs hybrids modified separator as efficient polysulfide barrier for high-performance lithium sulfur batteries. *Nano Res.* **2019**, *12*, 829–836. [[CrossRef](#)]
40. Li, P.Y.; Lv, H.W.; Li, Z.L.; Meng, H.P.; Lin, Z.; Wang, R.H.; Li, X.J. The Electrostatic Attraction and Catalytic Effect Enabled by Ionic-Covalent Organic Nanosheets on MXene for Separator Modification of Lithium-Sulfur Batteries. *Adv. Mater.* **2021**, *33*, 2007803. [[CrossRef](#)]
41. Hou, T.Z.; Chen, X.; Peng, H.J.; Huang, J.Q.; Li, B.Q.; Zhang, Q.; Li, B. Design Principles for Heteroatom-Doped Nanocarbon to Achieve Strong Anchoring of Polysulfides for Lithium-Sulfur Batteries. *Small* **2016**, *12*, 3283–3291. [[CrossRef](#)]
42. Zeng, P.; Huang, L.W.; Zhang, X.L.; Zhang, R.X.; Wu, L.; Chen, Y.G. Long-life and high-areal-capacity lithium-sulfur batteries realized by a honeycomb-like N, P dual-doped carbon modified separator. *Chem. Eng. J.* **2018**, *349*, 327–337. [[CrossRef](#)]
43. Pei, C.B.; Li, J.D.; Lv, Z.Z.; Wang, H.M.; Dong, W.; Yao, Y.Y. Inhibiting polysulfides with PDA/PEI-functionalized separators for stable lithium-sulfur batteries. *Int. J. Energy Res.* **2021**, *46*, 10099–10110. [[CrossRef](#)]
44. Zhang, H.; Lin, C.; Hu, X.H.; Zhu, B.K.; Yu, D.S. Effective Dual Polysulfide Rejection by a Tannic Acid/Fe(III) Complex-Coated Separator in Lithium-Sulfur Batteries. *ACS Appl. Mater. Interfaces* **2018**, *10*, 12708–12715. [[CrossRef](#)]
45. Liu, N.; Wang, L.; Tan, T.Z.; Zhao, Y.; Zhang, Y.G. TiO<sub>2</sub>/GO-coated functional separator to suppress polysulfide migration in lithium-sulfur batteries. *Beilstein J. Nanotechnol.* **2019**, *10*, 1726–1736. [[CrossRef](#)]
46. Xu, G.Y.; Yan, Q.B.; Wang, S.T.; Kushima, A.; Bai, P.; Liu, K.; Zhang, X.G.; Tang, Z.L.; Li, J. A thin multifunctional coating on a separator improves the cyclability and safety of lithium sulfur batteries. *Chem. Sci.* **2017**, *8*, 6619–6625. [[CrossRef](#)]
47. Bhargava, A.; He, J.; Gupta, A.; Manthiram, A. Lithium-Sulfur Batteries: Attaining the Critical Metrics. *Joule* **2020**, *4*, 285–291. [[CrossRef](#)]
48. Cheng, P.; Guo, P.Q.; Liu, D.Q.; Wang, Y.R.; Sun, K.; Zhao, Y.G.; He, D.Y. Fe<sub>3</sub>O<sub>4</sub>/RGO modified separators to suppress the shuttle effect for advanced lithium-sulfur batteries. *J. Alloys Compd.* **2019**, *784*, 149–156. [[CrossRef](#)]
49. Lv, X.; Lei, T.; Wang, B.; Chen, W.; Jiao, Y.; Hu, Y.; Yan, Y.; Huang, J.; Chu, J.; Yan, C.; et al. An Efficient Separator with Low Li-Ion Diffusion Energy Barrier Resolving Feeble Conductivity for Practical Lithium–Sulfur Batteries. *Adv. Energy Mater.* **2019**, *9*, 1091800. [[CrossRef](#)]
50. Zhao, M.; Peng, H.J.; Zhang, Z.W.; Li, B.Q.; Chen, X.; Xie, J.; Chen, X.; Wei, J.Y.; Zhang, Q.; Huang, J.Q. Activating Inert Metallic Compounds for High-Rate Lithium-Sulfur Batteries through In Situ Etching of Extrinsic Metal. *Angew. Chem.* **2019**, *58*, 3779–3783. [[CrossRef](#)]
51. Zhang, H.Y.; Dai, R.Q.; Zhu, S.; Zhou, L.Z.; Xu, Q.J.; Min, Y.L. Bimetallic nitride modified separator constructs internal electric field for high-performance lithium-sulfur battery. *Chem. Eng. J.* **2022**, *429*, 132454. [[CrossRef](#)]
52. Hong, X.J.; Song, C.L.; Yang, Y.; Tan, H.C.; Li, G.H.; Cai, Y.P.; Wang, H.X. Cerium Based Metal-Organic Frameworks as an Efficient Separator Coating Catalyzing the Conversion of Polysulfides for High Performance Lithium-Sulfur Batteries. *ACS Nano* **2019**, *13*, 1923–1931. [[CrossRef](#)] [[PubMed](#)]
53. Peng, L.; Yu, Z.J.; Zhang, M.K.; Zhen, S.Y.; Shen, J.H.; Chang, Y.; Wang, Y.; Deng, Y.F.; Li, A.J. A novel battery separator coated by a europium oxide/carbon nanocomposite enhances the performance of lithium sulfur batteries. *Nanoscale* **2021**, *13*, 16696–16704. [[CrossRef](#)] [[PubMed](#)]
54. Wang, Z.; Feng, M.; Sun, H.; Li, G.R.; Fu, Q.; Li, H.B.; Liu, J.; Sun, L.Q.; Mauger, A.; Julien, A.M.; et al. Constructing metal-free and cost-effective multifunctional separator for high-performance lithium-sulfur batteries. *Nano Energy* **2019**, *59*, 390–398. [[CrossRef](#)]
55. Lin, H.L.; Zhang, S.L.; Zhang, T.R.; Cao, S.; Ye, H.L.; Yao, Q.F.; Zheng, G.W.; Lee, J.Y. A Cathode-Integrated Sulfur-Deficient Co<sub>9</sub>S<sub>8</sub> Catalytic Interlayer for the Reutilization of “Lost” Polysulfides in Lithium-Sulfur Batteries. *ACS Nano* **2019**, *13*, 7073–7082. [[CrossRef](#)]

56. Song, S.L.; Shi, L.Y.; Lu, S.C.; Pang, Y.C.; Wang, Y.K.; Zhu, M.; Ding, D.W.; Ding, S.J. A new polysulfide blocker-poly(acrylic acid) modified separator for improved performance of lithium-sulfur battery. *J. Membr. Sci.* **2018**, *563*, 277–283. [[CrossRef](#)]
57. Chiu, L.L.; Chung, S.H. Composite gel-polymer electrolyte for high-loading polysulfide cathodes. *J. Mater. Chem. A* **2022**, *10*, 13719–13726. [[CrossRef](#)]
58. Li, D.D.; Yang, J.F.; Xu, X.; Wang, X.W.; Chen, J.T.; Xu, J.; Zhao, N. Synergistic inhibitory effect of ultralight CNTs-COOH@Fe<sub>3</sub>O<sub>4</sub> modified separator on polysulfides shuttling for high-performance lithium-sulfur batteries. *J. Membr. Sci.* **2020**, *611*, 118300. [[CrossRef](#)]
59. Wang, J.T.; Zhai, P.F.; Zhao, T.K.; Li, M.J.; Yang, Z.H.; Zhang, H.Q.; Huang, J.J. Lamina MXene-Nafion-modified separator with highly inhibited shuttle effect for long-life lithium-sulfur batteries. *Electrochim. Acta* **2019**, *320*, 134558. [[CrossRef](#)]
60. Zhang, T.Z.; Huang, J.Q.; Peng, H.J.; He, L.Y.; Cheng, X.B.; Chen, C.M.; Zhang, Q. Rational Integration of Polypropylene/Graphene Oxide/Nafion as Ternary-Layered Separator to Retard the Shuttle of Polysulfides for Lithium-Sulfur Batteries. *Small* **2016**, *12*, 381–389. [[CrossRef](#)]
61. Xu, R.; Sun, Y.Z.; Wang, Y.F.; Huang, J.Q.; Zhang, Q. Two-dimensional vermiculite separator for lithium sulfur batteries. *Chin. Chem. Lett.* **2017**, *28*, 2235–2238. [[CrossRef](#)]
62. Saroha, R.; Heo, J.; Li, X.Y.; Angulakshmi, N.; Lee, Y.; Ahn, H.J.; Ahn, J.H.; Kim, J.H. Asymmetric separator integrated with ferroelectric-BaTiO<sub>3</sub> and mesoporous-CNT for the reutilization of soluble polysulfide in lithium-sulfur batteries. *J. Alloys Compd.* **2022**, *893*, 162272. [[CrossRef](#)]
63. Yim, T.; Han, S.H.; Park, N.H.; Park, M.S.; Lee, J.H.; Shin, J.; Choi, J.W.; Jung, Y.J.; Jo, Y.N.; Yu, J.S.; et al. Effective Polysulfide Rejection by Dipole-Aligned BaTiO<sub>3</sub> Coated Separator in Lithium-Sulfur Batteries. *Adv. Funct. Mater.* **2016**, *26*, 7817–7823. [[CrossRef](#)]
64. Babu, D.B.; Giribabu, K.; Ramesha, K. Permselective SPEEK/Nafion Composite-Coated Separator as a Potential Polysulfide Crossover Barrier Layer for Li-S Batteries. *ACS Appl. Mater. Interfaces* **2018**, *10*, 19721–19729. [[CrossRef](#)]
65. Maletti, S.; Podetti, S.; Oswald, S.; Giebeler, L.; Barbero, C.A.; Balach, J. LiV<sub>3</sub>O<sub>8</sub>-Based Functional Separator Coating as Effective Polysulfide Mediator for Lithium-Sulfur Batteries. *ACS Appl. Energy Mater.* **2020**, *3*, 2893–2899. [[CrossRef](#)]
66. Ghazi, Z.A.; He, X.; Khattak, A.M.; Khan, N.A.; Liang, L.B.; Iqbal, A.; Wang, J.X.; Sin, H.; Li, L.S.; Tang, Z.Y. MoS<sub>2</sub>/Celgard Separator as Efficient Polysulfide Barrier for Long-Life Lithium-Sulfur Batteries. *Adv. Mater.* **2017**, *29*, 1606817. [[CrossRef](#)]
67. Chang, Z.; Qiao, Y.; Wang, J.; Deng, H.; Zhou, H.S. Two-dimensional metal-organic framework with perpendicular one-dimensional nano-channel as precise polysulfide sieves for highly efficient lithium-sulfur batteries. *J. Mater. Chem. A* **2021**, *9*, 4870–4879. [[CrossRef](#)]
68. Huang, Y.C.; Yen, Y.J.; Tseng, Y.H.; Chung, S.H. Module-Designed Carbon-Coated Separators for High-Loading, High-Sulfur-Utilization Cathodes in Lithium-Sulfur Batteries. *Molecules* **2021**, *27*, 228. [[CrossRef](#)]
69. Wu, S.L.; Shi, J.Y.; Nie, X.L.; Yao, Y.M.; Jiang, F.; Wei, Q.F.; Huang, F.L. Microporous Cyclodextrin Film with Funnel-type Channel Polymerized on Electrospun Cellulose Acetate Membrane as Separators for Strong Trapping Polysulfides and Boosting Charging in Lithium-Sulfur Batteries. *Energy Environ. Mater.* **2022**. [[CrossRef](#)]
70. Pei, H.J.; Yang, C.Y.; Wu, Q.Y.; Zhou, X.P.; Xie, X.L.; Hwang, B.; Ye, Y.S. Ion-selective aramid nanofiber-based Janus separators fabricated by a dry-wet phase inversion approach for lithium-sulfur batteries. *J. Mater. Chem. A* **2022**, *10*, 5317–5327. [[CrossRef](#)]
71. Sun, J.; Mu, Q.; Kimura, H.; Murugadoss, V.; He, M.; Du, W.; Hou, C.X. Oxidative degradation of phenols and substituted phenols in the water and atmosphere: A review. *Adv. Compos. Hybrid Mater.* **2022**, *5*, 627–640. [[CrossRef](#)]
72. Guo, Y.; Li, J.; Pittcheri, R.; Zhu, J.H.; Wen, P.; Qiu, Y.J. Electrospun Ti<sub>4</sub>O<sub>7</sub>/C conductive nanofibers as interlayer for lithium-sulfur batteries with ultra long cycle life and high-rate capability. *Chem. Eng. J.* **2019**, *355*, 390–398. [[CrossRef](#)]
73. Wang, X.B.; Luo, Y.H.; Wang, H.Y.; Wu, C.C.; Zhang, Z.S.; Lia, J.D. Tow-dimensional metal organic framework decorated porous carbon fiber as efficient interlayer for lithium-sulfur battery. *J. Electroanal. Chem.* **2021**, *897*, 115564. [[CrossRef](#)]